RESEARCH ARTICLE | AUGUST 14 2006

Electric-field-induced quenching of photoluminescence in photoconductive organic thin film structures based on Eu^{3+} complexes ⊘

J. Kalinowski; W. Stampor; M. Cocchi; D. Virgili; V. Fattori
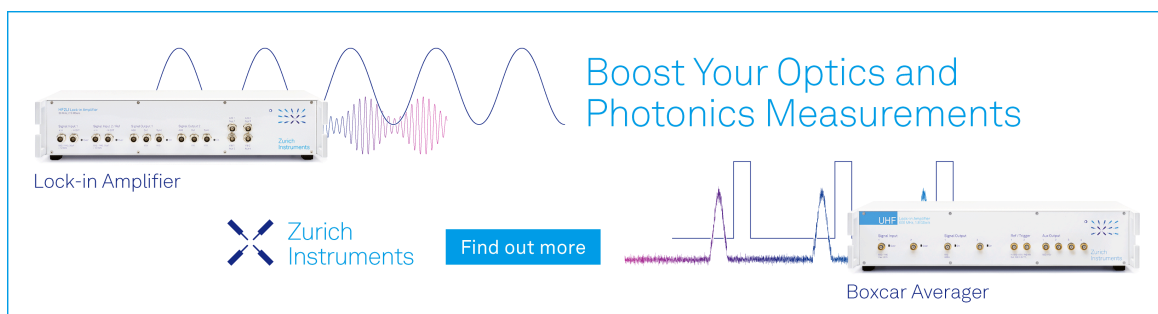
Check for updates

View Online

Export Citation

16 May 2024 13:18:24

Electric-field-induced quenching of photoluminescence in photoconductive organic thin film structures based on Eu^{3+} complexes

J. Kalinowski[a)] and W. Stampor
Department of Molecular Physics, Gdańsk University of Technology, 80-952 Gdańsk, Poland

M. Cocchi, D. Virgili, and V. Fattori
Institute of Organic Synthesis and Photoreactivity, National Research Council of Italy, (CNR-ISOF), I-40129 Bologna, Italy

A large electric field effect on photoluminescence (PL) from electroluminescent emitters sandwiched between two high-work-function electrodes is reported and a model of the effect formulated. We examine the PL behavior of Eu^{3+} complex-based organic thin films subjected to increasing electric field applied to either two high-work-function [indium tin oxide (ITO) and Au] or two low-work-function (Al/Al) electrodes. The progressive drop (up to 40%) of the PL for the first structure is observed while the current increases by about two orders of magnitude under illumination within the first absorption band of diamine derivative (TPD) molecules acting as an antenna harvesting exciting photons within the common matrix bonded with polycarbonate. This behavior is interpreted in terms of a field-dependent branching between ligand occupation by excited triplets and by electrons injected from negatively biased ITO or Au electrodes by TPD excitons. In contrast, the PL quenching in the Al/organic film/Al structure is due to exciton dissociation solely. This allows to extract the quenching component for the ITO/organic film/Au structure, associated with the injected charge only. The recombination of thermally injected holes with exciton-injected electrons makes the charge-induced quenching efficiency component to nonmonotonically evolve with a decrease down to negative values (PL enhancement) at high electric fields. The quenching of the emission from host (TPD) is attributed to singlet-exciton–charge-carrier interactions. © *2006 American Institute of Physics.* [DOI: 10.1063/1.2229577]

I. INTRODUCTION

The physical principles of operation of organic light-emitting diodes (LEDs) are founded on formation and decay mechanisms of excited states subjected to high electric fields applied to thin organic films using electrodes ensuring the efficient injection of holes and electrons.[1] One of the most significant problems facing electroluminescent (EL) devices is the quantum efficiency roll-off with a rate progressing for high drive current densities (high electric fields) operating LEDs. Three competing processes lead to nonradiative decay of emissive states-and thus to the observed EL quantum efficiency roll-off:[2–8] (i) mutual exciton-exciton annihilation,[2,3] (ii) electric-field-assisted dissociation of localized excited states and/or their precursors,[4] and (iii) interaction of excited states with charge carriers injected and distributed in some way in the emitter bulk.[1,3] All of them can occur in both electrofluorescent and electrophosphorescent organic LEDs, though, due to the long triplet lifetime, their role in electrophosphorescent LEDs is expected to be more pronounced. Efforts to improve the efficiency of electroluminescent emission should therefore concentrate on minimizing rates of these processes. Their mutual rate ratio is of great importance in determining the ways to reach this goal taking into account the device structure and its application purpose. However, it is hard to disentangle processes (i)–(iii) from electrical and optical characteristics of organic LEDs due to

the physical complexity of their operation mechanisms. The photoluminescence (PL) response to increasing excitation intensity has been recently used to infer various parameters describing excitonic interactions in electric-field-free thin organic films used as EL emitters.[1,6–9] The effect of exciton-exciton annihilation on the EL quantum efficiency of organic LEDs can be deduced from the relation between the critical excitation light intensity and its electrical equivalent of the critical current density (j_{crit}) at which exciton-exciton interactions become the process controlling the exciton lifetime.[7,8] The resulting values of j_{crit} (>0.5 A/cm^2) appeared to exceed the experimental data for organic LEDs by more than one order of magnitude. This strongly suggests processes (ii) and (iii) to be involved in the high-field EL quantum efficiency roll-off. In order to investigate them, a noninjecting and only one sign charge injecting electrodes must be provided to the organic emitters.

The purpose of this work is to study the effect of electric field on PL of thin solid organic films sandwiched between a pair of low-work-function Al/Al (non injecting) and high-work-function indium tin oxide (ITO)/Au (only hole injecting) electrodes, the structures expected to practically exclude the electron-hole recombination producing EL. A series of Eu^{3+} organic complex-based EL emitters has been used as an example. Unlike the Al/Eu^{3+} emitter/Al structure, the ITO/Eu^{3+} emitter/Au structure appeared to be highly photoconductive. The experimental results have shown that a straightforward combination of the field-assisted dissociation of localized excited states [process (ii)], underlying the PL

[a)]Author to whom correspondence should be addressed; electronic mail: kalino@polnet.cc
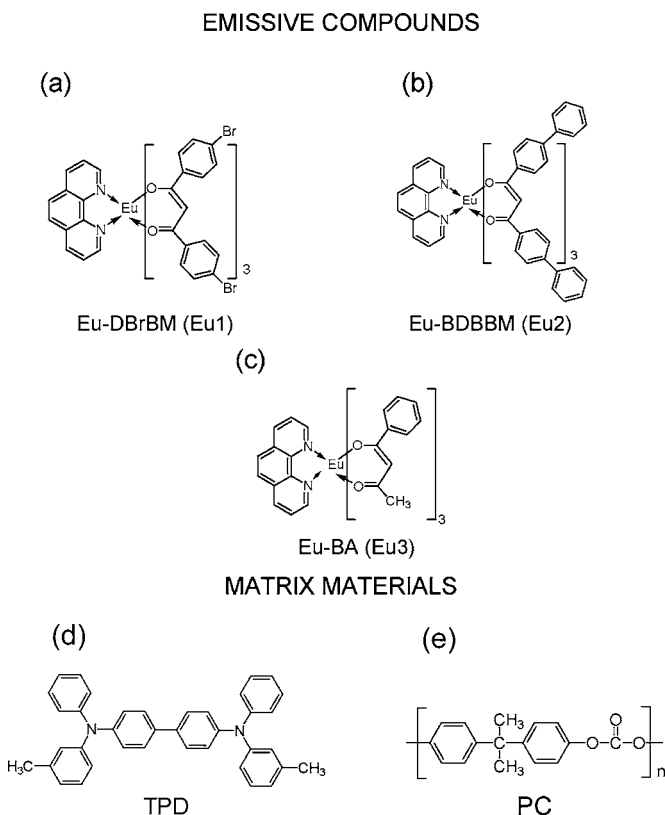
EMISSIVE COMPOUNDS

FIG. 1. The molecular structures of materials used. Luminophors: (a) (Eu1) Eu(BrBM)$_3$phen-tris[di(bromo)benzoylmethane]mono(phenathroline) europium(III), (b) (Eu2) Eu(BDBBM)$_3$phen-tris(biphenoylmethane)mono(phenathroline)europium(III), and (c) (Eu3) Eu(BABBM)$_3$phen-tris (benzoylacetonato)mono(phenathroline)europium(III). The different coligands (L$_1 \rightarrow$BrBM, L$_2 \rightarrow$BDBBM, L$_3 \rightarrow$BABBM) were chosen to examine the coligand role for the EPLQ. Matrix materials: (d) (TPD) N,N'-diphenyl-N,N'-bis(3-methylphenyl)-[1,1'-biphenyl]-4,4' diamine and (e) (PC) bisphenol-A-polycarbonate.
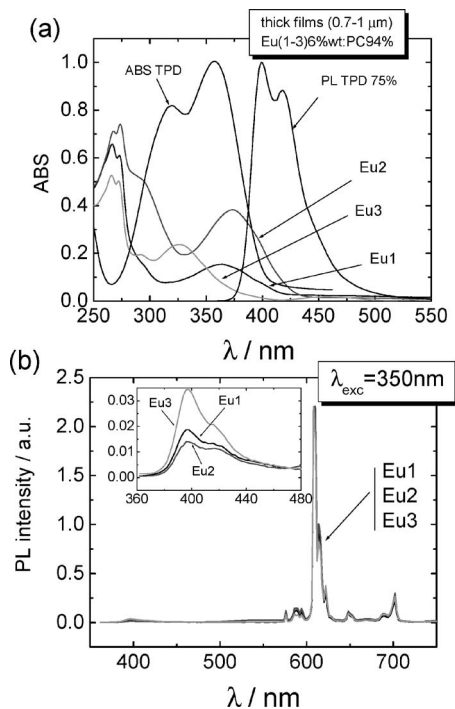

FIG. 2. Absorption (a) and emission spectra of host (TPD) and guest (Eu complexes: Eu1 to Eu3) materials used [(a) and (b)]; the absorption spectrum of TPD taken with a 100-nm-thick neat film and its emission spectrum for a [75 wt % TPD:PC] solid film (a) to be compared with the short-wavelength emission of 6% Eu(1–3)-doped (74% TPD:20% PC) 150-nm-thick films excited at λ_{exc}=350 nm as shown in (b). Left-upper corner inset in part (b): enlarged short-wavelength part of the emission spectra of four samples.

nonmonotonic evolution and even negative values (an enhancement) of the charge-induced quenching component as confirmed by experiment.

II. EXPERIMENT

Experiments were performed with 6 wt % Eu^{3+}-complexes-doped blends of N,N'-diphenyl-N,N'-bis (3-methylphenyl)-1,1'-biphenyl-4,4' diamine (TPD) and bisphenol-A-polycarbonate (PC). Three Eu^{3+}(L$_1$–L$_3$) phen complexes with the common ligand of phenathroline (phen) and four different coligands (L$_1$,L$_2$,L$_3$) were used as emissive dopants. The Eu^{3+} complexes to be abbreviated as Eu1 (with coligand L$_1$), Eu2 (L$_2$) and E3 (L$_3$) were purchased from SANDS Corp., TPD from Aldrich, and PC of molecular weight of 32 000–36 000 from Polysciences Inc., all used as supplied. The molecular structures of the materials used are shown in Fig. 1. The thicknesses of Eu^{3+}-complexes-doped layers, spun coat or cast using a precision doctor blade technique from a 10 mg/ml dichloromethane solution onto precleaned glass or quartz substrates, ranged between 70 and 170 nm and varied with film compositions. A special set of TPD-free samples of thicknesses between 0.7–1 μm was fabricated to characterize absorption properties of Eu^{3+} complexes themselves. They are displayed in Fig. 2 along with the emission spectra of all three Eu^{3+} complexes in (74% TPD:20% PC) host matrix. Typically, the emission spectra of Eu^{3+}-complex-doped films are dominated by the Eu complex emission decaying on sub-

quenching in the low-work-function electrodes structure alone, and their collision quenching with charge carriers [process (iii)] is unable to explain the observed strong PL quenching effects with the high-work-function electrodes structure, and an additional mechanism of the electric-field-induced PL modulation must have been involved.[10] In this article we formulate a simple model of the PL quenching in thin films subjected to external electric fields applied to the high-work-function electrodes structure. The PL output in this model is largely controlled by the field-dependent effective population of ligands acting as the energy transmitting species from the excited states of the matrix to the emissive Eu^{3+} cations, the latter standing for the complex center. The accessible ligand population decreases with applied field due to their occupation by electrons injected by matrix excitons from a negatively biased electrode, either ITO or Au. The large number of the exciton-injected electrons at the cathode transforms the monopolar hole-injection current in the dark into a much larger double-injection space-charge-limited current in the sample under illumination. Moreover, the exciton-injected electrons can recombine with injected holes, producing an additional amount of light, which in turn reduces the overall quenching process of the PL. The model predicts the
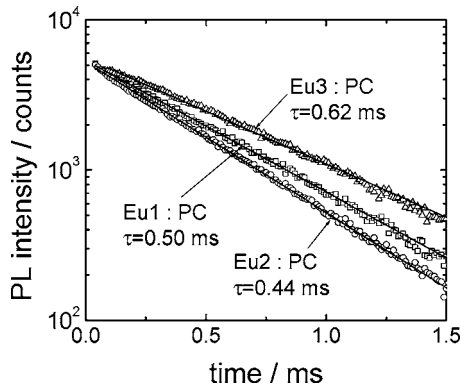
FIG. 3. PL decay of a thick (~ 1 μm) Eu1- to Eu3-doped PC films. The solid lines represent a monoexponential decay function with the average metal-centered excited state ($^5D_0$) lifetimes τ, as indicated in the figure.

FIG. 5. The general sample structure (a), glass/ITO transmittance spectrum (b) to be used in the exact determination of the charge photogeneration efficiency (note that 70% of the exciting radiation at 350 nm used enters the organic layer), and an example of the typical PL response to the DC ITO$^+$/Au$^-$-biased voltage for a glass/ITO/Eu2:TPD:PC (120 nm)/Au structure (c). The PL variation for five different voltages is given in (c). A nearly 30% reduction of the PL intensity at $U=15$ V ($F=1.25\times10^6$ V/cm) is seen, the initial PL level being restored after the 10 s field application time.

milliseconds scale and revealing a very narrow PL spectrum peaking at 610 nm [Fig. 2(b)]. The observed quasimonoexponential PL decay (Fig. 3) excludes bimolecular processes such as exciton-exciton interactions to participate in the relaxation of the excited states. The latter, being underlain by strongly bounded electronic configurations of the Eu^{3+} ion,[11] are effectively shielded from the influence of external factors including other Eu^{3+} ions and external electric fields. Thus, the present results on their lifetime and spectral behavior are similar to the literature data for other lanthanide metal complexes.[3,12–14] The negligibly weak features around 400 nm, due to the emission of host molecules of TPD, are seen in the PL spectra and a relatively stronger emission band between 500 and 550 nm, occurring pronouncedly in the electroluminescence spectra.[15] It might be associated with the phosphorescence of coligands, suggesting the TPD-transported holes to recombine on coligand-located electrons. In the example of Eu3, shown in Fig. 4, it corresponds well to the triplet state energy level of dibenzoylmethanato (DBM) ligand.[16]

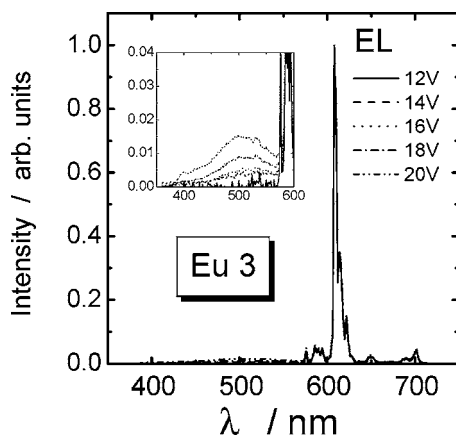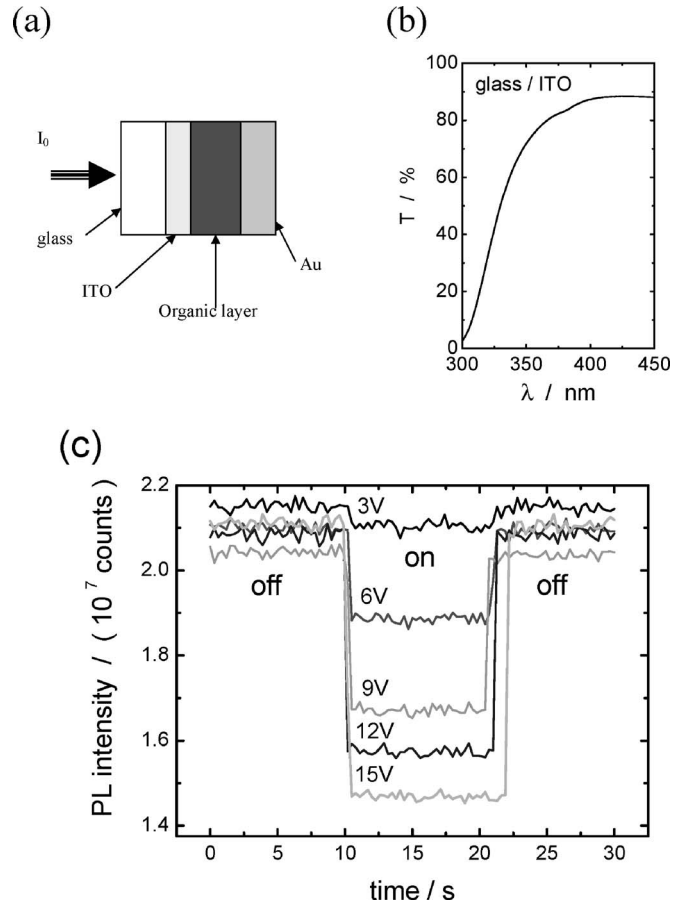The front$\rightarrow$ITO and nonsubstrate Al$\leftarrow$ face excited PL

FIG. 4. The electroluminescence (EL) spectrum of a Eu3-doped emitter containing TPD-hole transporting molecules from a double-layer LED with 2-(biphenyl-4-yl)-5-(4-butylphenyl)-1, 3, 4 oxadiazole (PBD) electron-transporting layer, provided with the ITO hole- and Ca-electron injecting electrodes at different applied voltages (given in the figure). The enlarged residual emission features from host (TPD) molecules ($\sim$400 nm) and DBM coligand (500–550 nm) are shown in the inset.

of organic structures (A)$\rightarrow$glass/ITO/6% Eu(1–3):74% TPD:20% PC(150–170 nm)/Au and (B) quartz/Al/6% Eu(1–3): 74%TPD:20% PC(70–100 nm)/Al$\leftarrow$, respectively, were studied. These structures were characterized via (i) the current-field dependence, recorded with a Keithley source measure unit, (ii) the photocurrent action spectra and its intensity dependence using a Spex Fluorolog 2 spectrofluorimeter and a Keithley source unit, and (iii) the PL output as a function of dc and ac applied fields.

Electromodulation of the PL in structure (A) was performed by applying a progressively increasing dc voltage and taking an average PL intensity over a time of 10 s before (Φ_0) and after (Φ) the voltage rise step for each value of the voltage (Fig. 5). The PL intensity was sampled every 0.3 s with a Spex Fluorolog 2 spectrofluorimeter, the results displayed by either the ratio $\delta=[\Phi_0-\Phi(F)]/\Phi_0$ or $\delta'=[\Phi_0-\Phi(F)]/\Phi(F)$ as function of electric field (F) within the emission ranges corresponding to the weak host fluorescence of TPD ($\lambda_{max}\cong420$ nm) and strong guest emission of Eu^{3+} ion ($\lambda_{max}\cong610$ nm) (see emission spectra in Fig. 2). The PL from structure (B) was modulated by a sinusoidal field as described elsewhere.[17] The second Fourier harmonic of the
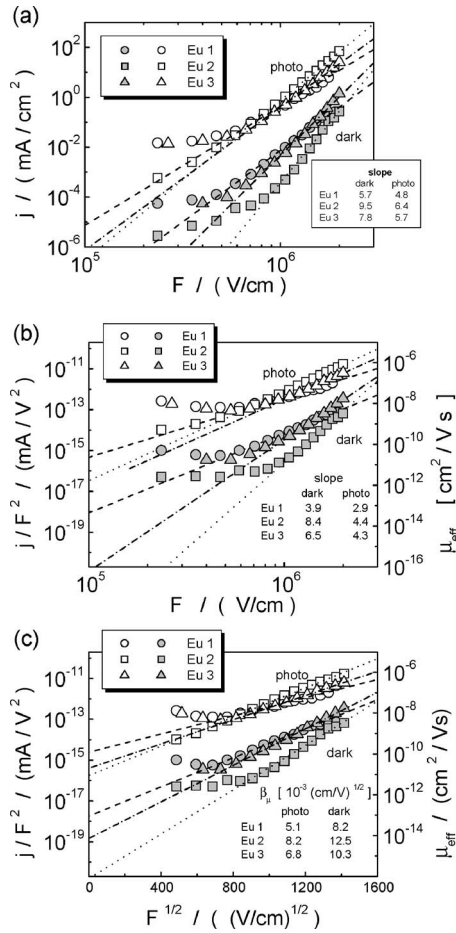
FIG. 6. Current–electric-field characteristics of structure (A) taken in the darkness (filled points) and under illumination (photo) through the ITO anode (open points) in the $\log j$-$\log F$ (a) and $\log(j/F^2)$-$F^{1/2}$ (b) representations. Photocurrents were generated with light of $\lambda_{exc}=350$ nm and intensity $I_0=7\times10^{14}$ quanta/cm^2 s. The straight lines are high-field fits to the data assuming SCLC conditions in $\mu(F)=$const (a) and $\theta(F)=$const (b) approximations. Their slopes give characteristic parameters for the approximations used. μ_{eff} on the right-hand ordinate stands for the effective mobility calculated as $\mu_{eff}\cong\theta\mu=jd/\varepsilon_0\varepsilon F^2$ (for details see Sec. IV).

modulated PL signal was transformed into the steady-state quenching ratio δ to be compared with that for structure (A). The measurements for structure (A) were carried out at 295 K and under argon atmosphere, whereas the structure (B) samples were kept in ambient atmosphere at room temperature.

III. RESULTS

The dependence of the dark-current and photo current flows in structure (A) on the external applied field ($F=U/d$, where U is the applied voltage and d is the organic layer thickness) is shown in Fig. 6 as plotted in two different representations corresponding to two space-charge-limited-current (SCLC) approximations discussed in Sec. IV. In the high-field limit both the dark-current and photocurrent approach well the SCLC behavior which would imply the photocurrent (j_{ph}) to be light intensity (I_0) independent. Indeed, up to 1.5×10^6 V/cm, practically I_0 independent photocurrent reveals only a very weak increase of j_{ph} with I_0 at the upper limit of the applied voltage, where j_{ph} tends to become
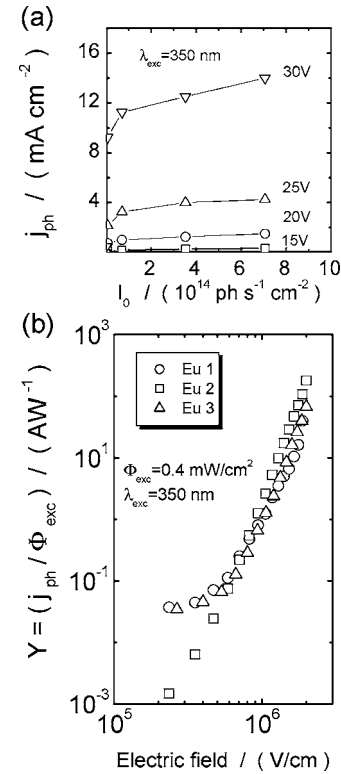

FIG. 7. Incident light intensity (I_0) dependence of the photocurrent (j_{ph}) at different voltages applied to the structure (A) with Eu3 emitter, →ITO/6 wt % Eu3:74% TPD:20% PC (150 nm)/Au (a). The photocurrent yield ($Y=j_{ph}/\Phi_{exc}$) vs the applied electric field for structure (A) with all three Eu(1–3) emissive molecules (b). The exciting power intensity (Φ_{exc}) and the exciting wavelength (λ_{exc}) are given in the figure.

an injection limited current like that within the low intensity excitation region for I_0 below 10^{13} photons/cm^2 s [Fig. 7(a)]. The important question is the origin of such a high photocurrent exceeding the dark current by at least one order of magnitude independent of the cell bias (either ITO positive or negative) [cf. Fig. 6(a)]. The bulk photogeneration of charge can be ruled out on the basis of the field-increasing photocurrent yield [Fig. 7(b)]. Defined as $Y=j_{ph}/\Phi_{exc}$ [A/W], it leads to the photogeneration efficiency $\eta=j_{ph}/eTI_0=(Y/eT)h\nu$ [e/photon] which with the photon energy $h\nu=3.54$ eV and glass/ITO transmittance $T=0.7$ at $\lambda_{exc}=350$ nm [see Fig. 5(b)], for all $Y>0.2$ A/W, that is, in the high-field regime, exceeds unrealistically its upper limit of unity. Excluding the photoenhancement of SCLC, as shown in Sec. IV we conclude that the measured j_{ph} is a result of a strong excitonic injection of electrons at the cathode (either negatively biased ITO or Au), transforming only hole SCL dark current into the double-injection SCLC under illumination.[1,18] The electron injection on the cathode by the hole space charge enhancement of the local field is to be neglected due to the high barrier for the thermionic electron injection to TPD from either ITO or Au cathode ($\Delta E_e \cong2.5$ eV, see, e.g., Ref. 19), consistent with not observing any light emission from these structures in the dark. We note that the TPD singlet-exciton energy E_S(TPD)$\cong2.9$ eV [see the fluorescence spectrum in Fig. 2(a)] matches quite well to this barrier ensuring proper energetic conditions for the excitonic injection of electrons while injection by TPD triplet
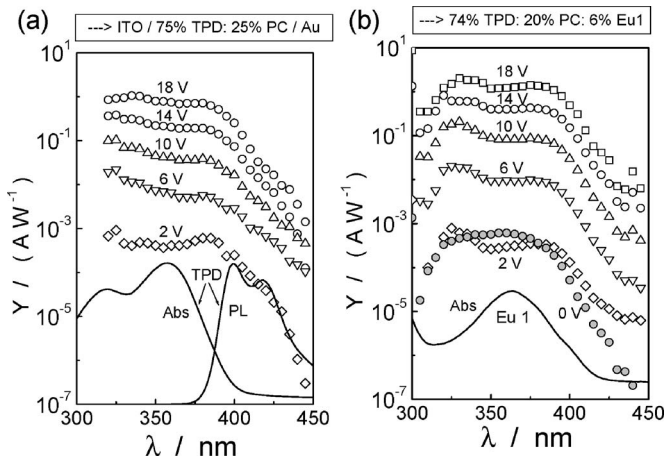
FIG. 8. Action spectra of the photocurrent yield (Y) for the matrix film structure ITO/75 wt % TPD:25 wt % PC/Au (a) and the Eu1-doped structure ITO/6 wt % Eu1:74 wt % TPD:20 wt % PC/Au (b). Unlike in the matrix film, a photocurrent at $U=0$ (photovoltaic current) occurs for structure (A) [part (b)].

exciton, $E_T \cong 2.3$ eV,[20] requires a finite activation energy. The leading role of TPD singlets in the photocurrent generation process follows from a comparison of the photocurrent in Eu^{3+}-complex-doped samples with that in the (TPD:PC) matrix itself. The action spectra of the photocurrent yield (Y) for these two different structures are shown in Fig. 8. Their almost flat shape within the (320–380 nm) wavelength range falls in the first absorption band of TPD, suggesting a similarity in the photocurrent generation process. The penetration depth of the exciting light within this spectral range varies between $l_a \cong 70$ and 130 nm (60 nm at $\lambda_{exc} = 350$ nm); thus the excitation of samples is more or less homogeneous, a weak antibatic feature of Y seen at $\cong 350$ nm, and apparent drop for $l_a \geqslant d = 150$–170 nm. Slightly higher values of Y and the occurrence of a photovoltaic current (at $U=0$) for structure (A) are associated with the presence of Eu complex.

The essential information is contained in Fig. 9 showing how the electric-field-induced PL output change (PL quenching δ) varies as a function of the field applied to structure (A) for all three Eu(1–3) complex-doped emitters studied and measurements performed with the residual emission originating from the matrix material TPD ($\lambda_{em} = 420$ nm) and the narrow-band emission from the dopants at $\lambda_{em} = 610$ nm (cf. the emission spectra in Figs. 2 and 4). While for the host emission the maximum PL quenching can be as low as 0.7% and does not exceed 10%, its values for the Eu3 guest emission reaches 40% and do not drop below 10%. We note the meaningful differences in the modulation depths of the host emission with the same amount of different dopants, particularly between Eu1- and Eu3-doped emitters.

Unlike structure (A), structure (B) reveals a low sensitivity to illumination. The net photocurrent is comparable or even smaller than already low dark current. Its linear increase with excitation intensity along with a superlinear field increase suggests the small amount of charge carriers to be produced by dissociation and decaying in monomolecular-type processes. Figure 10 shows the PL quenching δ as a function of applied electric field for different emitters underlying structure of type (B). The magnitude of δ reaches val-
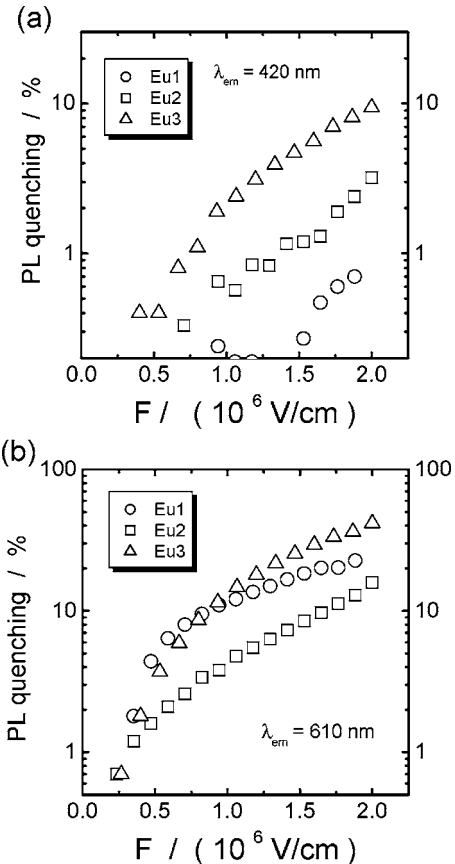

FIG. 9. PL (Φ) quenching, $\delta = [\Phi(0) - \Phi(F)]/\Phi(0)$, as a function of electric field applied to Eu(1–3)-doped film structures ITO/6% Eu(1,2;3):74% TPD:20% PC(170 nm; 150 nm)/Au, observed at the host TPD emission wavelength $\lambda = 420$ nm (a) and at the guest Eu emission wavelength $\lambda = 610$ nm (b). Excitation at wavelength $\lambda_{exc} = 350$ nm and intensity $I_0 = 7 \times 10^{14}$ photons/cm^2 s.

ues of 0.1–3% at 10^6 V/cm and slightly exceeds 10% for Eu-complex-doped samples at 2×10^6 V/cm. The absolute quenching of photoluminescence falls below the values obtained with experiments for similar structures containing neat films of Alq_3,[17,21] $Ir(ppy)_3$,[4] and TPD,[22] but their direct comparison does not provide any precise conclusion since the neat films have been excited with a large excess of photon energy with respect to their $S_0 \rightarrow S_1$ transition. As the only reason for exciton quenching at moderate excitation intensity in structure (B) is the electric-field-assisted dissociation of excited states, and the dissociation efficiency increases with increasing exciting photon energy in a manner difficult to define, any quantitative conclusion based on the confrontation of the electromodulation results must be drawn with a great caution. On the other hand, the electric field dependence of exciton dissociation can be successfully described in terms of Onsager theory of geminate recombination.[23] It assumes either initially excited vibrationally hot or relaxed excitons to dissociate into Coulombically bound electron-hole (e-h) pairs [geminate pairs (GP)], which can recombine to repopulate the localized excited state (emissive in luminescent materials) or fully dissociate into free charge carriers (or at least one mobile carrier). The dissociation efficiency (η), depending on the energy surplus upon excitation, is determined by diffusive Brownian motion of the charges within
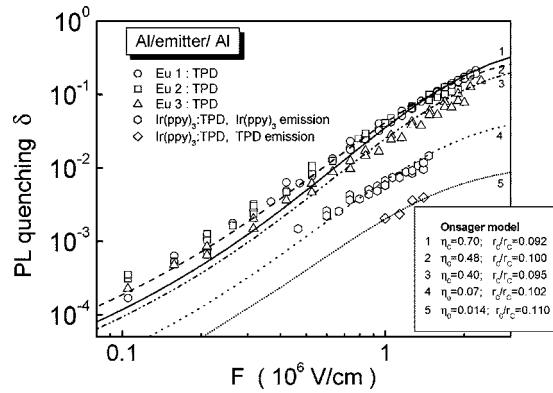
FIG. 10. PL (Φ) quenching, $\delta=[\Phi(0)-\Phi(F)]/\Phi(0)$, vs applied field in a number of thin film structures of type (B) with different emissive molecules: Eu1, Eu2, Eu3, and Ir(ppy)$_3$ [*fac* tris(2-phenyl-pyridine) iridium]. The effect observed for the residual emission of TPD (diamonds) at $\lambda_e\cong420$ nm, emissive Eu^{3+}-complex molecules ($\lambda_e\cong610$ nm), and Ir(ppy)$_3$ emission from the doped film [6 wt % Ir(ppy)$_3$:74 wt % TPD:20 wt % PC] is confronted with theoretical predictions of the Onsager model 1938 of geminate recombination (Ref. 23), as given by the curves from 1 to 5. The Onsager model parameters η_0 and r_0/r_c are given in the right-bottom inset.

the mutual Coulombic potential modified by an external electric field. The detailed mechanism by which GPs are created is still an open question, but using the Onsager formalism their initial distance r and yield η_0 can be determined. An inherent parameter of the Onsager theory is Onsager's radius $r_c=e^2/4\pi\varepsilon_0\varepsilon kT$, defined by the charge separation at which the energy of *e-h* Coulombic attraction, $e^2/4\pi\varepsilon_0\varepsilon r_c$, equals the kinetic energy of the carrier, kT. With typical dielectric constant $\varepsilon=3$, at room temperature, $r_c\cong20$ nm. Premised upon the applicability of Onsager's theory, the values of r/r_c and η_0 can be inferred from measurements of the PL quenching as a function of applied electric field,[24]

$$\delta(F)\cong\eta_{\text{Ons}}(F)=\eta_0\int g(r,\theta)f(r,\theta)d\tau. \qquad (1)$$

The electric field dependence occurs through the field-dependent probability that a GP with a separation distance r will escape geminate recombination, given by the Onsager function

$$f(r,\theta)=\exp[-(A+B)]\sum_m^\infty\sum_{n=0}^\infty\frac{A^m}{m!}\frac{B^{m+n}}{(m+n)!}, \qquad (2)$$

where $A=r_c/r$, $B=eFr(1+\cos\theta)/2KT$, and θ determines the orientation of the applied field with respect to the radius vector **r**. The function $g(r,\theta)$ expresses the probability per unit volume of finding the ejected carrier in a volume element $d\tau$ at (θ,r) for the specific ionization process. Assuming that $g(r,\theta)$ is spherically symmetric and independent of F, it can be approximated by a δ function,

$$g(r)=\delta(r-r_0)/4\pi r_0^2, \qquad (3)$$

with a discrete value of the initial separation distance $r=r_0$. All the field dependence experimental plots of the PL quenching (figure points) presented in Fig. 10 could be reasonably well reproduced by the Onsager theory 1938 (lines), using function (3) with a similar value of $r_0/r_c\cong0.1$ but η_0 varying from 0.7 for the sample with emissive Eu1 down to

0.014 for the emission component of TPD. This would suggest the quenching of the emission of dopant to be a result of the combined dissociation of excited singlets of host TPD and guest emissive molecules, consistent with an enhancement of the photocurrent yield and the occurrence of photovoltaic effect with the doped samples (Fig. 8). Clearly, the much stronger PL quenching in structure (A) (Fig. 9) must be underlain by additional mechanisms imposing the PL reduction. They are discussed in Sec. IV.

IV. DISCUSSION

From the experimental results, it is obvious that the phenomena responsible for the PL quenching in structure (A) with high-work-function electrodes (ITO/Au) are different from those underlying the PL quenching in structure (B) with low-work-function electrodes (Al/Al). While the latter can be rationalized by the dissociation of the excited states of the host (TPD) and guest [Eu^{3+} complexes and Ir(ppy)$_3$] molecules only (see Sec. III), the role of the injected charge must be taken into account to explain the large electric-field-imposed PL changes in structure (A).

A. Charge injection

The decrease of the PL yield and the simultaneous occurrence of high photoconduction in structure (A) can consistently be interpreted on the premise of thermionic hole and excitonic electron injection from high-work-function electrodes of ITO and Au. An analysis of the field (F) evolution of the current (j) flowing through the structure in the dark and under illumination (photo) in the high-field regime ($F>0.8$ MV/cm) shows both to bear out either a power-law behavior $j\sim F^n$ [Figs. 6(a) and 6(b)] or a product of two field-increasing functions, $j\sim F^2\exp(\beta_\mu F^{1/2})$ [Fig. 6(c)]. They are indicative of space-charge-limited currents (SCLCs), $j\cong\varepsilon_0\varepsilon\theta\mu F^2/d$, where θ is the free-to-total carrier concentration ratio, μ is the microscopic carrier mobility, and d is the film thickness. The straight-line segments of the log j-log F plots in Fig. 6(a) represent the $\mu(F)=$const SCLC approximation with the field-dependent $\theta\cong(N_{\text{eff}}/H^l)n^{l-1}$ for an exponential energy (E) distribution of localized traps $h(E)=(H/lkT)\exp(-E/lkT)$, where N_{eff} is the effective density of states, H is the total concentration of traps, l is their characteristic energy distribution parameter, and $n\cong\varepsilon_0\varepsilon F/ed$ is the total concentration of charge.[18] This leads to the current equation $j\cong(\varepsilon_0\varepsilon\mu N_{\text{eff}}/H^ld)(\varepsilon_0\varepsilon/ed)^{l-1}F^{l+1}$; the log-log plot is expected to be a straight line with the slope $(l+1)$ as observed in Fig. 6(a). The straight-line segments of the $\log(j/F^2)-\log F$ [Fig. 6(b)] and $\log(j/F^2)-F^{1/2}$ [Fig. 6(c)] plots reflect another SCLC approximation that assumes the current to obey the Child law ($j\sim F^2$) modified by the effective field-dependent mobility $\mu'=\theta\mu$. The field dependence of $\mu'(F)$ can be rationalized on the trap spatial correlation concept assuming either the traps to be correlated by the randomly distributed strains due to the physical and chemical imperfections of the material (macrotraps[25]) or the correlation imposed by the averaging of charge-dipole interactions in polar charge-transporting media [correlated dipolar disorder model[26] (CDDM)]. In the mac-

rotrap model, transport occurs through hops among spatially extended domains (macrotraps) characterized by the strain imposed spatial distribution of local states, $E(r) = (3kT/\sigma_m)\ln(r_0/r)$, where $E(r)$ is the energy of a microscopic state located at a distance r from the center of one type of spherical symmetry macrotraps of radius r_0. Here, σ_m is the scaling factor of the exponential energy distribution of local states (microtraps), $h(E) = (H_0\sigma_m/kT)\exp(-\sigma_m E/kT)$, of the total concentration H_0. The macrotrap model predicts the effective (one carrier) high-field mobility to be a power function of F,[25]

$$\mu' \cong \mu \frac{N_{\text{eff}}}{N_0}\left(\frac{2.7\sigma_m e r_0 F}{3kT}\right)^{3/\sigma_m}\exp(-\varepsilon_t/kT), \quad (4)$$

where N_0 is the concentration of macrotraps and ε_t is the macrotrap depth. The microscopic mobility $\mu(F) = \text{const.}$

The CDDM treats carrier hopping among local sites arranged on a cubic lattice of cell spacing a, the carriers interacting with randomly oriented dipole molecules placed at each lattice site. The many long-range contributions introduce correlations described by the function $C(r) \sim \sigma_d a/r$ which decays slowly with intersite separation r. Here, $\sigma_d = 2.35ep/\varepsilon_0\varepsilon a^2$ is the rms width of the dipolar energetic disorder dependent on the dipole moment p. In the CDDM, the field dependence of the nondispersive mobility is characterized by a Poole-Frenkel-type function[26]

$$\mu(F) = \mu(F=0)\exp\beta_\mu F^{1/2}, \quad (5)$$

with

$$\beta_\mu = \frac{0.78}{kT}\left[\sigma_d - (kT)^2\frac{\Gamma}{\sigma_d}\right]\left(\frac{ea}{kT}\right)^{1/2}, \quad (6)$$

where $\mu(F=0)$ is the zero-field mobility and Γ characterizes geometrical disorder.

Though it is insufficient to conclude which of these two approximations is obeyed, both of them are underlain by the charge concentration being proportional to the field strength F. Noting the difference in the slopes for j_{ph} and j_{dark} in both approximations, straight-line plots in Figs. 6(a)–6(c), a plausible explanation for j_{ph} is efficient injection of electrons by TPD excitons from the negatively biased electrode (either ITO or Au). The current becomes the double-injection current exceeding largely the unipolar hole-injection current in the dark. The assignment of j_{ph} to the photoenhanced current,[18] $j_{\text{ph}} \sim I_0^{1-1/l}$, fails, because the high value of $l \cong 6$ would lead to the relatively strong exciting light intensity (I_0) dependence $j_{\text{ph}} \sim I_0^{0.8}$ at variance with experiment showing a much weaker dependence of the photocurrent on I_0 [Fig. 7(a)]. Also, this rules out the current controlled by interface photoinjection which would generate a linear current-excitation intensity dependence. The double injection, generating a bimolecular recombination current in the samples, would explain the observed weak dependence of j_{ph} on wavelength (λ) and intensity of the exciting light, varied between 325–390 nm and 10^{13}–10^{15} photons/cm^2 s at $\lambda = 350$ nm, respectively (Figs. 7 and 8). The mobility μ_{eff} in the equation for double-injection current represents, in general, a combination of electron (μ_e) and hole (μ_h) mobilities

as well as the recombination mobility $\mu_0 = \varepsilon_0\varepsilon\gamma_{eh}/2e$—a quantity bearing the mobility dimension and balancing the current with the recombination component through the second order electron-hole recombination rate constant γ_{eh}.[1,18] The one-segment high-field increase of $\log(j/F^2)$ plots seems to indicate the photocurrent to obey the strong-recombination limit case ($\mu_{\text{eff}} \cong \mu_e + \mu_h \cong \mu_h$). In this approximation the recombination current component is large ($\mu_e, \mu_h \ll \mu_0$) and $\mu_h \gg \mu_e$ Hence, μ_{eff} can be replaced by $\mu_h \cong \mu_h\theta$ as given in Eq. (4) or (5) with $\mu = \mu_h$ and $\beta_\mu = \beta_{\mu h}$. To fully discuss the observed current behavior with electric field, we also have to consider the alternative weak-recombination limit ($\mu_e, \mu_h \gg \mu_0$), the so-called plasma case, leading to[1]

$$\mu_{\text{eff}} \cong \frac{2}{3}\mu_h\left(\frac{2\pi\mu_e}{\mu_0}\right)^{1/2}$$
$$= \frac{2}{3}\mu_{0h}\left(2\pi\frac{\mu_{0e}}{\mu_0}\right)^{1/2}\exp\left[\frac{2\beta_{\mu h} + \beta_{\mu e}}{2}F^{1/2}\right], \quad (7)$$

the slopes in Fig. 6(c) stand then for $\beta_\mu = (2\beta_{\mu h} + \beta_{\mu e})/2$. It must be here pointed out that the requirement $\mu_e, \mu_h \gg \mu_0$ does not withstand the assumption $\mu_h \gg \mu_e$ if the recombination process is described in the Langevin formalism [$\gamma_{eh} = (e/\varepsilon_0\varepsilon)(\mu_e + \mu_h)$].

B. PL quenching

In our previous paper[10] the conceptual framework has been laid down for a qualitative understanding of the large PL quenching imposed by electric field applied to Eu^{3+}-complex-based organic thin film emitters provided with two high-work-function electrodes. It has been proposed that the overall PL quenching δ is a combination of three processes: (a) electric-field-assisted dissociation of both host and guest excited states, (b) exciton-charge-carrier interaction upon their collision, and (c) the charge-occupation control of the effective concentration of ligands acting as the energy transmission species between light harvesting TPD host molecules and the emissive complex center, the cation Eu^{3+}. Here, we intend to give a more detailed description of this concept aimed at a quantitative study of the observed effects.

The differential equation governing the steady-state concentration S_{host} of TPD singlets in the presence of an external electric field F can be approximated by

$$\dot{S}_{\text{host}}(F) = \alpha I_{\text{exc}}[1 - \eta_{\text{host}}(F)] - k_{\text{tot}}^{(\text{host})}(F)S_{\text{host}}(F) = 0, \quad (8)$$

where $\alpha I_{\text{exc}}[1 - \eta_{\text{host}}(F)]$ is the generation rate of host singlet excitons related directly to the linear absorption coefficient α and intensity I_{exc} of exciting light and $[1 - \eta_{\text{host}}]$ stands for the probability of the excited states to avoid dissociation characterized by its field and exciting photon energy ($h\nu$) dependent efficiency $\eta_{\text{host}}(F, h\nu)$. The term $k_{\text{tot}}^{(\text{host})} = k_r + \gamma_{\text{tr}}N + \gamma_{Sq}n_f + \gamma_{Sq}^{(t)}n_t + k_{\text{nr}}$ represents all monomolecular radiative (k_r) and nonradiative decay rate constants including the energy transfer (γ_{tr}) to available ligands ($N = N_0 - n$) populated by the concentration of complex dopant (N_0) and occupied partly by the injected charge of concentration n_t and nonra-

diative relaxation to lower excited states (e.g., triplet or ground state) as well as quenching on the interfaces (predominantly on the metallic electrodes) (k_{nr}). The TPD excitons (S_{host}) can be quenched by either free ($\gamma_{Sq}n_f$) and trapped [$\gamma_{Sq}^{(t)}n_t$] charge carriers. It should be noted that Eq. (8) assumes quenching processes (b) and (c) to operate on relaxed S_1 excitons, while process (a) occurs at a time shorter than their lifetime, possibly from excitonic precursor states generated on the exciting light absorption stage consistent with recent time-resolved fluorescence quenching and charge photogeneration studies.[27,28] In addition, the triplet energy transfer TPD→ligands has been assumed to be negligible due to the energy barrier between their excited triplets ΔE_T $\cong 0.44$ eV [E_T(TPD)$\cong 2.3$ eV (Ref. 20) and E_T(phen) $\cong 2.74$ eV (Ref. 29)]. Possible energy transfer from the triplets produced by the intersystem crossing on the ligands to TPD contributes to the nonradiative decay pathways of the excited ligand triplets along with the efficient energy supply to the emissive Eu³⁺ ions[30] (see discussion later on).

The solution of Eq. (8), $S_{host}(F)=\alpha I_{excl}[1-\eta_{host}(F)]/k_{tot}(F)$, allows to relate the PL at $F=0$ (Φ_0) to the PL at $F\neq 0$ [$\Phi(F)$] as

$$\delta'_{host} = \frac{S_{host}(F=0)}{S_{host}(F)} - 1 = \frac{\delta'_{q(host)}}{1-\eta_{host}(F)} + \delta'_{dis(host)}$$
$$\cong \delta'_{q(host)} + \delta'_{dis(host)}, \qquad (9)$$

where

$$\delta'_{q(host)} = \frac{[\gamma_{Sq}^{(t)}-\gamma_{tr}]n_t + \gamma_{Sq}n_f}{k_{tot}(F=0)} \qquad (10)$$

and

$$\delta'_{dis(host)} = \frac{\eta_{host}(F)}{1-\eta_{host}(F)} \cong \eta_{host}(F) \qquad (11)$$

are the quenching components imposed by charge carriers and by dissociation, respectively. The approximations made in Eqs. (9) and (11) are based on the data of Fig. 10 (curve 5) providing experimental and theoretical dependence of $\delta_{dis(host)}$ for the host emission of TPD and showing $\eta_{host}(F)$ $\ll 1$ within the entire range of applied electric fields. Once having the dissociation component, the charge quenching component can be calculated from the measured overall quenching effect, according to Eq. (9). Note that any δ' $\rightarrow\infty$ at total quenching conditions defined as $\delta=[\Phi_0-\Phi(F)]/\Phi_0=1$. This might be confusing for the *quenching* notion but allows the overall electric field modulation effect to be expressed as a simple sum (9). To fall in the intuitively understood PL quenching range, $0\leq\delta\leq1$, δ' can be simply translated into $\delta=\delta'/(1+\delta')$, but δ_{host} is no more the sum of the two components δ_q and δ_{dis}, unless one deals with weak quenching effects when $\delta'\ll1$ and $\delta\cong\delta'$. This is the case with the PL quenching of the host emission of TPD apparent in Figs. 9 and 10.

Basing on the above brief analysis, the δ_q component of the overall quenching δ for the TPD emission can be extracted. Its field dependence is shown in Fig. 11. All the measured δ-F curves clearly manifest their nonlinearity [Fig.
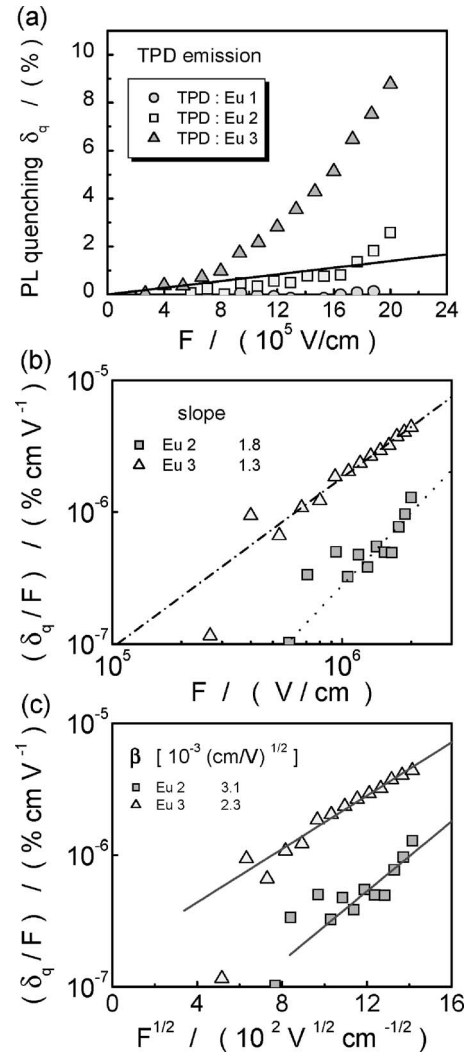

FIG. 11. The field dependence of the charge-induced host (TPD) PL quenching component, δ_q, for three (Eu1-, Eu2-, and Eu3-doped) samples, in different representations: (a) linear δ_q-F plot, (b) log(δ_q/F)-log F scale, and (c) log(δ_q/F)-$F^{1/2}$ scale. The nonlinear $\delta_q(F)$ increase (a) is interpreted in terms of the macrotrap model predicting straight-line plots log(δ_q/F) vs log F (b) or CDDM predicting the straight-line plots log(δ_q/F) vs $F^{1/2}$ (c) (cf. Sec. IV A).

11(a)] indicating both trapped and free carriers to participate in the quenching process [see Eq. (10)]. The superlinear increase of δ with field comes from the field-increasing electron and hole mobilities (cf. Sec. IV A). From the general expression for the current flowing inside the film, j $=e(\mu_h n_h+\mu_e n_e)F$, the concentration of more mobile free holes, $n_f\cong n_h\cong j/e\mu_h F$, can be derived, assuming $\mu_h n_h$ $\gg\mu_e n_e$. Since the photocurrent has been identified as the double-injection SCLC ($j\cong\varepsilon_0\varepsilon\mu_{eff}F^2/d$, cf. Sec. IV A) with μ_{eff} given by either Eq. (4) and (5), the concentration of free holes follows $n_h\cong\varepsilon_0\varepsilon\mu_{eff}F/ed\mu_h$ which when inserted into Eq. (10) gives electric field modulation of the PL:

$$\delta'_{q(host)} = \frac{[\gamma_{Sq}^{(t)}-\gamma_{tr}]\varepsilon_0\varepsilon}{edk_{tot}(F=0)}F + \frac{\gamma_{Sq}\varepsilon_0\varepsilon}{edk_{tot}(F=0)}$$
$$\times F\frac{N_{eff}}{N_0}\exp(-\varepsilon_t/kT)\left(\frac{2.7\sigma_m er_0 F}{3kT}\right)^{3/\sigma_m} \qquad (12)$$

for the macrotrap model and

TABLE I. Experimental and fit parameters to macrotrap and correlated dipolar disorder models of charge transport, taken from electrical (j_{dark}, j_{ph}) and PL quenching (δ_{PL}) characteristics.

Sample	a_{Eu} [a] (nm)	σ_m [b] From j_{ph}	σ_m [b] From δ_{PL}	σ_m^{dark}	β_μ [c] [10^{-3} (cm/V)$^{1/2}$]	s [d] [10^{-3} (cm/V)$^{1/2}$]	$\beta_{\mu e}$ [e] [10^{-3} (cm/V)$^{1/2}$]	$\beta_{\mu h}$ [e] [10^{-3} (cm/V)$^{1/2}$]	σ_e [e] (meV)	σ_h [e] (meV)	β_h^{dark} [10^{-3} (cm/V)$^{1/2}$]	σ_h^{dark} (meV)
Eu1	3.24	1.03	···	0.26	5.1	···	···	···	···	···	8.2	114
Eu2	3.23	0.68	0.97	0.77	8.2	3.1	6.2	5.1	254	83	12.5	174
Eu3	2.66	0.70	1.30	0.46	6.8	2.3	4.6	4.5	207	75	0.3	144

[a]Calculated from a_{Eu} (nm)$=10^7 (M/c\rho N_A)^{1/3}$ with the guest concentration $c=6$ wt %, assumed sample material density $\rho=1.2$ g/cm^3, Avogadro's number $N_A=6\times10^{23}$/mol, and molecular weight M(Eu1)$=1475$ g/mol, M(Eu2)$=1457$ g/mol, and M(Eu3)$=815$ g/mol.

[b]Calculated from slopes ($3/\sigma_m$) of the high-field straight-line plot segments in Figs. 6(b) and 11(b) or j_{ph} and δ_{PL}, respectively.

[c]From j_{ph}.

[d]From δ_{PL}.

[e]From δ_{PL} and j_{ph}. σ_e calculated from Eq. (6) with $a=0.76a_{Eu}$, $\Gamma=0$ and $kT=250$ meV; σ_h (also later σ_h^{dark}) with the same Γ and kT but with $a=0.78a_{TPD}$ $=0.78$ nm ($a_{TPD}\cong1$ nm).

$$\delta'_{q(host)} = \frac{[\gamma_{Sq}^{(t)} - \gamma_{tr}]\varepsilon_0\varepsilon}{edk_{tot}(F=0)}F$$
$$+ \frac{2}{3}\frac{\varepsilon_0\varepsilon\theta}{edk_{tot}(F=0)}\gamma_{Sq}\left(2\pi\frac{\mu_{0e}}{\mu_0}\right)^{1/2}F\exp\left(\frac{\beta_{\mu e}}{2}F^{1/2}\right) \tag{13}$$

for the CDDM.

Equations (12) and (13) explain the observed nonlinearity of the field increase of the host emission quenching [Fig. 11(a)]. The low-field linear increase represented by the first term becomes gradually dominated by the power in (12) or exponentially in (13) increasing function of electric field as shown in Figs. 11(b) and 11(c). The slopes of the high-field straight-line plots $\log(\delta'/F) - \log F$ and $\log(\delta'/F) - F^{1/2}$ provide the powers $3/\sigma_m$ and $s=\beta_{\mu e}/2$ exponential factors, respectively; the latter combined with β_μ slopes from Fig. 6(c) allow to determine $\beta_{\mu e}=2s$ and $\beta_{\mu h}=(2\beta_\mu-\beta_{\mu e})/2=\beta_\mu-s$. All these parameters are summarized in Table I. It clearly shows substantial differences in the dark current (j_{dark}), photocurrent (j_{ph}), and PL quenching (δ_{PL}) response to the field evolution of the charge injected into samples. The lower values of σ_m^{dark}, as compared with σ_m obtained from j_{ph} and δ_{PL}, indicate a light-induced deepening of the macrotraps, the largest effect seen for the PL quenching. An explanation could be the elimination of the low energetic edge of the holes trapped in the neighborhood of electrons. But a more probable alternative is that in contrast to the dark current, involving by definition the entire interelectrode space, the j_{ph} (recombination current) and δ_{PL} occur in selected regions of the sample bulk, characterized by a deeper macrotraps on average. This would be consistent with the location of the recombination zone close to the negatively biased electrodes, where structural and chemical perturbations of the sample are expected to emerge most efficiently. The same holds for the CDDM interpretation. The larger dipolar disorder parameter σ_d for holes (σ_h) extracted from the dark-current data (σ_m^{dark}) than that extracted from the j_{ph} and δ_{PL} measurements (σ_h) can be related to different sample regions. As expected σ_e exceeds substantially σ_h, since the weak electron transport occurs between dopant molecules more than two times distant as compared with the intermolecular spacing of TPD-

hole transporting material. A relatively large value of σ_m^{dark} requires a relatively large value of the dipole moment, $p \cong 5-6.5$ D (obtained with $\varepsilon=3-4$, see Sec. IV A), exceeding three to four times the dipole moment of TPD molecules, p(TPD)$\cong1.5$ D.[31] Therefore, the effect of higher-polarity dopants on the overall dipolar correlation must be taken into account to make the CDDM applicable to the interpretation of the present results. The correspondence between decreasing macrotrap potential gradient (or weakening spatial correlations) and the observed increase in the PL quenching by charge for Eu^{3+} complexes with the [(acac)CH$_3$ph] (Eu3) coligand is borne out by Table I. It seems to be a natural consequence of the increasing mobilities in the quenching regions (not seen in the current) assumed to be responsible for the PL quenching process [see Eq. (10)]. On the first glance the effect could be associated with decreasing molecular weight of the dopants, but electronic properties (e.g., dipole moment) of coligands might contribute to the δ_q increase for Eu3.

In contrast to the monotonously field-increasing δ_q for the emission of TPD host material, the charge component quenching (δ_q) extracted from the overall PL quenching effect (δ), observed on the Eu^{3+} ion emission from the dopant, shows, in addition, a nonmonotonic behavior with a broad maximum or minimum as shown in Fig. 12 for Eu1 and Eu2. The rate equation governing the steady-state concentration of N_{guest} excited states [(Eu^{3+})*] is

$$\dot{N}_{guest} = \gamma_{tr}[(1-f)N_0 - n][1 - \eta_{guest}(F)]S_{host} + \frac{j(1-\eta_{CP})}{ed}$$
$$- k_{tot}^{(guest)}N_{guest} = 0. \tag{14}$$

Here, the first (generation) term is due to the energy transfer from optically generated host singlets (S_{host}) to accessible ligands with their concentration $N(F)=[(1-f)N_0-n]$ reduced with respect to the dopant molecular concentration (N_0) by the field (current)-dependent charge occupation (n) of the ligands and possible dopant aggregation, the latter accounted for by the aggregation factor f. The energy transfer is effective only to the fraction $[1-\eta_{guest}(F)]$ of the guest emissive states which avoided the initial dissociation process with
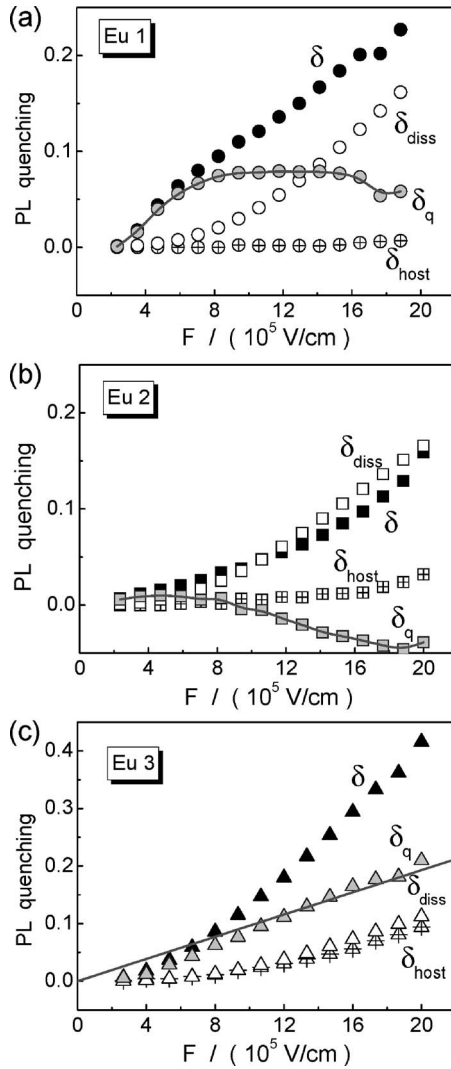
FIG. 12. Comparison of the total, $\delta_{\text{guest}} \equiv \delta$, dissociation component, $\delta_{\text{dis(guest)}} \equiv \delta_{\text{diss}}$, and charge-induced component, $\delta_{q\text{(guest)}} \equiv \delta_q$, PL quenching for the red Eu^{3+} emission from three Eu-complex-doped samples [Eu1 (a), Eu2 (b), and Eu3 (c)] selected by different field evolution of component δ_q. The total quenching of the host (TPD) emission, δ_{host}, is shown for completion the quenching picture. Solid lines are fits of δ_q to Eq. (16), $\delta_{q\text{(guest)}}$ $= C_1 F - C_2(1 - \eta_{\text{CP}})j$, using the $j(F)$ characteristics from Fig. 6(a) and $\eta_{\text{CP}}(F)$ as given in Fig. 13. The following parameters have been used in the fitting procedure: Eu1: $C_1(1-f) = 3.3 \times 10^{-9}$ cm/V, $C_2(1-f) = 1.3 \times 10^5$ cm^2/A; Eu2: $C_1(1-f) = 3.3 \times 10^{-9}$ cm/V, $C_2(1-f) = 7.3 \times 10^4$ cm^2/A; and Eu3: $C_1(1-f) = 2.1 \times 10^{-9}$ cm/V, $C_2 = 0$.

$\eta_{\text{guest}}(F)$ being their field-assisted dissociation efficiency. The second term, being proportional to the current density (j), takes into account the direct generation of the guest excited states due to the recombination of mobile holes with *phen*-located electrons. Only a fraction $(1 - \eta_{\text{CP}})$ of such charge pair (CP) precursors leads to the effective phen triplets because of their electric-field-increasing dissociation efficiency η_{CP}. The third term of (14) describes the decay rate of the guest emissive states with $k_{\text{tot}}^{\text{(guest)}} = k_{\text{r}}^{\text{(guest)}} + k_{\text{nr}}^{\text{(guest)}}$ standing for the field-independent decay rate constant for the radiative $[k_{\text{r}}^{\text{(guest)}}]$ and nonradiative $[k_{\text{r}}^{\text{(guest)}}]$ monomolecular processes. From a first order approximation of the solution of Eq. (14), the quenching ratio of the guest luminescence, δ_{guest}, is as follows:

$$\delta_{\text{guest}}(F,j) \cong \delta_{\text{host}}(F) + \eta_{\text{guest}}(F) + \frac{n(F)}{(1-f)N_0}$$

$$- \frac{j(1 - \eta_{\text{CP}})}{ed(1-f)\alpha I_0}, \quad (15)$$

where αI_0 substitutes the product $\gamma_{\text{tr}}S_{\text{host}}(0)$ appearing in (14) for $F = 0$. It allows $\delta_{q\text{(guest)}}$ to be determined by the subtraction of $\delta_{\text{host}}(F)$ and $\eta_{\text{guest}}(F)$ components obtained from the independent measurements on structure (A) $[\delta_{\text{host}}(F)]$ and structure (B) $[\eta_{\text{guest}}(F)]$, which is given by

$$\delta_{q\text{(guest)}}(F,j) \cong \frac{n(F)}{(1-f)N_0} - \frac{j(1 - \eta_{\text{CP}})}{ed(1-f)\alpha I_0}. \quad (16)$$

In essence, Eq. (14) describes the steady-state kinetics for excited triplets of phen, but their population becomes faithfully reflected in the emission of $(\text{Eu}^{3+})^*$ states since Eu^{3+} ions take efficiently over the phen triplet energy. Equations (14)–(16) have been derived under the following premises: (i) the energy back transfer from excited Eu^{3+} ions to the ligands can be neglected [the metal-centered $^5D_0$ level of Eu^{3+} is well lower than the triplet state energy of phen, $\Delta E \cong 0.6$ eV (Ref. 30)], (ii) the field-assisted dissociation efficiencies fall much below unity (see Fig. 10), and (iii) the collision charge quenching of $(\text{Eu}^{3+})^*$ states is ineffective because $4f$ orbitals of the metal ion Eu^{3+} are effectively shielded from the influence of the external forces by the overlapping $5s^2$ and $5p^6$ shells, which imply the f^n configurations to be relatively insensitive to the external fields.[11]

The experimental data of $\delta_{q\text{(guest)}}$ shown in Fig. 12 illustrate an interplay between two terms of Eq. (16). It is apparent that the emissive state population losses can be balanced by their field-increasing increment due to the hole (TPD$^+$)-electron (phen$^-$) recombination. If the progressive formation of excited ligand triplets by the recombination process is negligible as compared with their population resulted from the energy transfer of optically generated S_{host} states, the contribution of the second term in (16) becomes insignificant and one would expect the q quenching of the guest emission, $\delta_{q\text{(guest)}}$, to be positive and increasing proportional to the concentration of phen-trapped electrons $[n(F)]$. This might be caused by a weak aggregation of the guest molecules $[(1-f) \rightarrow 1]$ and/or high excitation intensity I_0. Such a case seems to be realized with Eu3 [Fig. 12(c)]. From the slope, $\varepsilon_0\varepsilon/ed(1-f)$, of the linear plot $\delta_{q\text{(guest)}} - F$, $f \cong 0.98$ follows with $\varepsilon = 3$, indicating that a large majority of 98% of the dopant molecules undergoes the aggregation. In the case of Eu1 and Eu2 [Figs. 12(a) and 12(b)], the second term in (16) cannot be neglected, showing, in particular, their exact balance, $\delta_{q\text{(guest)}} = 0$, at $F \cong 0.8$ MV/cm and $\delta_{q\text{(guest)}} < 0$ above this field strength for Eu2. At this value of the field, at a given excitation wavelength ($\alpha \cong 7.2 \times 10^3$ cm^{-1}) and intensity ($I_0 \cong 7 \times 10^{14}$/cm^2 s) with $d = 170$ nm and $j \cong 0.22$ mA/cm^2, $n/N_0 \cong j(1 - \eta_{\text{CP}})/ed\alpha I_0 \cong 2 \times 10^{-3}$ which gives an idea about the electron occupation fraction of the total nominal concentration of phen ligands with the experimental conditions of the present study. On the other hand, a decrease of the always positive values of $\delta_{q\text{(guest)}}$, above $F \cong 0.8$ MV/cm, is observed with Eu1 [Fig. 12(a)]. The
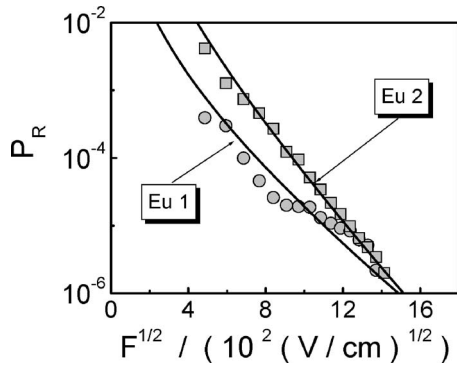
FIG. 13. The electric field dependence of the electron(phen$^-$)-hole(TPD$^+$) recombination probability, $P_R = 1 - \eta_{CP}$, as resulted from the fitting procedures in Fig. 12. The solid lines are fits to experimental data of Eq. (19) for Eu1- and Eu2-based emitters. The parameters used to calculate P_R are $p(\text{Eu1}) = 1.6 \times 10^3$ V/cm, $\beta_\mu = (\text{Eu1}) = 4.4 \times 10^{-3}$ (cm/V)$^{1/2}$, and $p(\text{Eu2}) = 3.3 \times 10^4$ V/cm and $\beta_h(\text{Eu2}) = 6.3 \times 10^{-3}$ (cm/V)$^{1/2}$.

smooth curves in Figs. 12(a) and 12(b) are calculated from Eq. (16) expressed as $\delta_{q(\text{guest})} = C_1 F - C_2(1 - \eta_{CP})j$; the fitting parameters $C_1 \cong \varepsilon_0 \varepsilon / ed(1-f)N_0$ and $C_2 \cong [ed(1-f)\alpha I_0]^{-1}$ are given in the figure captions. From their values $0.97 \leqslant f_{\text{Eu1}} < 1$ and $0.9 \leqslant f_{\text{Eu2}} < 1$ are evaluated with $\varepsilon = 3$ and $d = 170$ nm, close to $f_{\text{Eu3}} = 0.98$. Thus, they are not expected to govern the field behavior of the charge quenching component (δ_q). Instead, the types of traps and/or disorder would determine the shape of $\delta_q(F)$ through the field dependence of the electron (phen$^-$)-hole (TPD$^+$) recombination probability $P_R = 1 - \eta_{CP}$. The field dependence of P_R extracted from the fitting procedures of Fig. 12 is shown in Fig. 13. The probability P_R that the *e-h* pair recombines is

$$P_R = 1 - \eta_{CP} = (1 + \tau_c/\tau_{\text{diss}})^{-1} \cong \tau_{\text{diss}}/\tau_c. \tag{17}$$

Here, τ_c is the capture and τ_{diss} the dissociation time of the pair. The approximation in (17) has been made on the premise $P_R \ll 1$ as may be seen in Fig. 13. We assume the capture to be the final step in the recombination process for the carriers located on the nearest-neighbor sites ($r_{CP} \cong 2-3$ nm), where the intercarrier Coulombic field exceeds largely the applied (external) field strength. Thus, $\tau_c(F) = \text{const}$, but τ_{diss} for 2 nm $< r_{CP} < r_c \cong 20$ nm is affected by the external electric field and can be expressed as

$$\tau_{\text{diss}} = \langle r_{CP} \rangle / v_{\text{drift}} = \langle r_{CP} \rangle / \mu(F)F, \tag{18}$$

where $\langle r_{CP} \rangle$ is the average intercarrier spacing in CPs.

From this definition and with Eq. (5), one can determine the field dependence of P_R,

$$P_R(F) = [\langle r_{CP} \rangle / \tau_c \mu(0)F] \exp(-\beta_h F^{1/2}). \tag{19}$$

Its fit to the experimental data is shown in Fig. 13. The fitting parameters, $p = \langle r_{CP} \rangle / \tau_c \mu(0)$ and β_h, differ for Eu1- and Eu2-doped emitters. While the first one is $\cong 20$ times lower for Eu1- than for Eu2-doped emitter, β_h differs by a factor of 2 only. Using the fit values of β_h, $\sigma_d = 70 \pm 10$ meV for Eu1 and $\sigma_d = 100 \pm 10$ meV for Eu2 follow from Eq. (6) with $\Gamma = 0$ and $a = a_{\text{TPD}} = 1$ nm. This is in good agreement with σ_h calculated on the basis of current-field characteristics from Fig. 6 (cf. Table I). For these values of σ_d we then find $\mu(F=0)$ which,

according to the one-dimensional (1D) analysis of Ref. 32, is predicted to yield

$$\mu(F=0) = \mu^{(0)} \exp[-(\sigma_d/kT)^2], \tag{20}$$

where $\mu^{(0)}$ is the zero-field carrier mobility of disorder-free samples. Use of Eq. (20) allows the ratio $\mu(F=0) \times(\text{Eu2})/\mu(F=0)(\text{Eu1}) \cong 3 \times 10^{-4}$ to be evaluated. Since the experimental $p(\text{Eu1})/p(\text{Eu2})$ parameter ratio ($\cong 4.8 \times 10^{-2}$) is about two orders of magnitude larger than the above mobility ratio, its difference between Eu1- and Eu2-doped samples is expected to reflect a two order difference in the capture time τ_c (such a large difference in $\langle r_{CP} \rangle$ for these two samples is unjustified).

V. CONCLUDING REMARKS

We demonstrated large electric field effects on relative photoluminescence (PL) yield from Eu^{3+}-complex-doped thin film emitters sandwiched between two high-work-function electrodes, ITO/emitter/Au. Measurements of the electric-field-dependent PL quenching ratio, the dark and photocurrent field characteristics, and their comparison with similar data for the emitters sandwiched between two low-work-function electrodes (Al/emitter/Al) allow to extract quantitative information concerning nonradiative decays of the excited states of the fluorescent host material (TPD) and Eu^{3+} complex dopants. The results are in good agreement with the predictions of a kinetic model based upon the (i) coexistence of dissociation of excited states and their interactions with free and trapped charge carriers and (ii) trade-off between quenching of the Eu^{3+} excited states and their repopulation due to the recombination of thermally injected holes from a high-work-function anode and exciton-injected electrons from a high-work-function cathode.

The essential differences in the electric field evolution of the PL quenching for different coligand Eu^{3+}-phen complex emitters sandwiched between high-work-function electrodes have been observed. They reflect directly the varying dissociation-to-effective charge PL quenching component ratio in the overall electric field effect. While the electric field effect on the PL from the emitters provided with low-work-function electrodes is clearly due to the dissociation of excited states, the dominating role of the dissociation component in the high-work-function electrode film structure is somewhat surprising. This occurs whenever the charge quenching component becomes negative demonstrating the effective repopulation process of excited states in a recombination process. To gain a more fundamental understanding of charge quenching component, we have analyzed current (and photocurrent) field characteristics. The results show the PL quenching effects and electrical properties of the film structures to be underlain by differentiation of disorder parameters. The present study has been motivated in part by its presumed relevance to the functioning of organic light-emitting diodes.

ACKNOWLEDGMENTS

lar, supramolecular and macromolecular components with photonic and optoelectronic properties" and FIRB Project No. RBNE019H9K entitled "Nanometric machines through molecular manipulation."

[1] J. Kalinowski, *Organic Light Emitting Diodes: Principles, Characteristics, and Processes* (Dekker, New York, 2005).

[2] M. A. Baldo, S. Lamansky, P. E. Burrows, M. E. Thompson, and S. R. Forrest, Appl. Phys. Lett. **75**, 4 (1999).

[3] M. A. Baldo, C. Adachi, and S. R. Forrest, Phys. Rev. B **62**, 10967 (2000).

[4] J. Kalinowski, W. Stampor, J. Mężyk, M. Cocchi, D. Virgili, V. Fattori, and P. Di Marco, Phys. Rev. B **66**, 235321 (2002).

[5] M. Cocchi, V. Fattori, D. Virgili, C. Sabatini, P. Di Marco, M. Maestri, and J. Kalinowski, Appl. Phys. Lett. **84**, 1052 (2004).

[6] I. Sokolik, R. Priestley, A. D. Walter, R. Dorsinville, and C. W. Tang, Appl. Phys. Lett. **69**, 4168 (1996).

[7] J. Mężyk, J. Kalinowski, F. Meinardi, and R. Tubino, Chem. Phys. Lett. **395**, 321 (2004).

[8] J. Mężyk, J. Kalinowski, F. Meinardi, and R. Tubino, Appl. Phys. Lett. **86**, 111916 (2005).

[9] E. B. Namdas, A. Ruseckas, I. D. Samuel, S.-C. Lo, and P. L. Burn, Appl. Phys. Lett. **86**, 091104 (2005).

[10] D. Virgili, M. Cocchi, V. Fattori, J. Kalinowski, and W. Stampor, Appl. Phys. Lett. **88**, 051102 (2006).

[11] G. A. Crosby, Mol. Cryst. **1**, 37 (1966).

[12] M. D. Mc Gehee, T. Bergstedt, C. Zhang, A. P. Saab, M. B. O'Regan, G. C. Bazan, V. I. Srdanov, and A. J. Heeger, Adv. Mater. (Weinheim, Ger.) **11**, 1349 (1999).

[13] H.-G. Liu, Y.-I. Lee, S. Park, K. Jang, and S. S. Kim, J. Lumin. **110**, 11 (2004).

[14] C. Yang *et al.*, Angew. Chem., Int. Ed. **43**, 5010 (2004).

[15] J. Kalinowski, W. Stampor, M. Cocchi, D. Virgili, and V. Fattori, Appl. Phys. Lett. **86**, 241106 (2005).

[16] H. J. Kim, J. E. Lee, Y. S. Kim, and N. G. Park, Opt. Mater. (Amsterdam, Neth.) **21**, 181 (2002).

[17] W. Stampor, J. Kalinowski, P. Di Marco, and V. Fattori, Appl. Phys. Lett. **70**, 1935 (1997).

[18] W. Helfrich, in *Physics and Chemistry of the Organic Solid State*, edited by D. Fox, M. M. Labes, and A. Weissberger (Wiley, New York, 1967), Chap. 1.

[19] Y. Ohmori, H. Kajii, T. Sawatami, H. Ueta, and K. Yoshino, Thin Solid Films **393**, 407 (2001).

[20] M. A. Baldo and S. R. Forrest, Phys. Rev. B **62**, 10958 (2000).

[21] J. Szmytkowski, W. Stampor, J. Kalinowski, and Z. H. Kafafi, Appl. Phys. Lett. **80**, 1465 (2002).

[22] W. Stampor, Chem. Phys. **256**, 351 (2000).

[23] L. Onsager, Phys. Rev. **54**, 554 (1938).

[24] M. Pope and C. E. Swenberg, *Electronic Processes in Organic Crystals* (Clarendon, Oxford, 1982), pp. 481–497.

[25] J. Kalinowski, J. Godlewski, P. Di Marco, and V. Fattori, Jpn. J. Appl. Phys., Part 1 **31**, 818 (1992).

[26] S. V. Novikov, D. H. Dunlap, V. M. Kenkre, P. E. Parris, and A. V. Vannikov, Phys. Rev. Lett. **81**, 4472 (1998).

[27] D. Hertel, E. V. Soh, H. Bässler, and L. J. Rothberg, Chem. Phys. Lett. **361**, 99 (2002).

[28] V. Gulbinas, Y. Zaushitsyn, V. Sundström, D. Hertel, H. Bässler, and A. Yartsev, Phys. Rev. Lett. **89**, 107401 (2002).

[29] S. Quici *et al.*, Inorg. Chem. **41**, 2777 (2002).

[30] O. L. Malta, H. F. Brito, J. F. S. Menezes, F. R. Gonçalves e Silva, C. de Mello Donegá, and S. Alves, Jr., Chem. Phys. Lett. **282**, 233 (1998).

[31] R. H. Young and J. J. Fitzgerald, J. Phys. Chem. **99**, 4230 (1995).

[32] D. H. Dunlap, P. E. Parris, and V. M. Kenkre, Phys. Rev. Lett. **77**, 542 (1996).